DESIGN OF A 130 MW AXIAL TURBINE OPERATING WITH A SUPERCRITICAL CARBON DIOXIDE MIXTURE FOR THE SCARABEUS PROJECT

Abdelrahman Abdeldayem[1], Salma Salah[1], Omar Aqel[1], Martin White[1,2], Abdulnaser Sayma[1]

[1]Thermo-Fluids Research Centre, School of Mathematics, Computer science and Engineering, City, University of London. EC1V 0HB, United Kingdom

[2]Thermo-Fluid Mechanics Research Centre, School of Engineering and Informatics, University of Sussex, Brighton, BN1 9RH, United Kingdom

ABSTRACT

The application of supercritical carbon dioxide (sCO_2) mixtures in power generation cycles could improve power block efficiency for concentrated solar power applications. Mixing CO_2 with titanium tetrachloride ($TiCl_4$), hexafluoro-benzene (C_6F_6), sulphur dioxide (SO_2) or others increases the critical temperature of the working fluid, allowing it to condense at ambient temperatures in dry solar field locations. Therefore, transcritical power cycles, which have lower compression work and higher thermal efficiency compared to supercritical cycles, become feasible. This paper presents the flow path design of a utility-scale axial turbine operating with an 80-20% molar mix of CO_2 and sulphur dioxide (SO_2). A preliminary turbine design has been developed for the selected mixture using an in-house mean-line design code considering both mechanical and rotor dynamic criteria. Furthermore, 3D blades have been generated and blade shape optimisation has been carried out for the first and last turbine stages of the multi-stage design. It has been found that increasing the number of stages from 4 to 14 stages increase the total-to-total efficiency by 6.3%. The final turbine design has a total-to-total efficiency of 92.9% as predicted by the 3D numerical results with maximum stress less than 260 MPa and a mass flow rate within 1% of the intended cycle mass-flow rate. Optimum aerodynamic performance was achieved with a 14-stages design where the hub radius and the flow path length are 310 mm and 1800 mm respectively.

KEYWORDS

AXIAL TURBINE, SUPERCRITICAL CARBON DIOXIDE, MEAN-LINE DESIGN, BLADE SHAPE OPTIMISATION

INTRODUCTION

Supercritical carbon dioxide power cycles (sCO_2) are promising candidates for concentrated solar power (CSP) plants [1, 2]. sCO_2 power cycles operate between two pressure limits where both the heat addition and heat rejection pressures are higher than the critical point of the working fluid. Consequently, the compression process takes place in the supercritical phase. The EU funded SCARABEUS project [3] is investigating the applicability of transcritical power cycles operating with CO_2-mixtures, where the working fluid is compressed in the liquid phase. This could result in enhanced power generation efficiency and bring the levelised cost of electricity (LCoE) of CSP plants to a competitive level within the renewable energy market [4]. Therefore, several sCO_2 based mixtures have been proposed to increase the mixture's

critical temperature, and hence allow for air condensation in a transcritical power cycle for dry regions where water cooling is not available [3, 5].

According the study presented by Escanta et al. [6], blending CO_2 with carbonyl sulfide (COS) increased the efficiency of the cycle to 45.05%, compared to 41.25% for pure CO_2, while the cost of electricity decreased to 2621 \$/kWe compared to 2811 \$/kWe for pure CO_2. The SCARABEUS consortium [3] has proposed hexafluorobenzene (C_6F_6), sulfur dioxide (SO_2), and titanium tetrachloride ($TiCl_4$) as possible mixtures [7, 8]. The effects of changing C_6F_6 and $TiCl_4$ molar fractions on cycle performance were presented considering safety and health characteristics [9, 10]. The study revealed an absolute efficiency gain of 3% compared to pure CO_2 cycles, whilst the optimum mixture molar fraction ranged from 10% to 20%. The cycle layouts were also simpler when using mixtures compared to pure CO_2 cycles. Doping pure CO_2 with 20% to 30% SO_2 was investigated by Crespi et al. [8] which resulted in an optimised recompression cycle with an efficiency of 51% at 700 ℃.

The SCARABEUS consortium has tested the thermal stability of the three candidate mixtures for operation at a turbine inlet temperature of 700 ℃. According to the test results, titanium tetrachloride ($TiCl_4$) does not thermally degrade at 700 ℃. On the contrary, C_6F_6 shows signs of thermal degradation for temperatures above 600-625 ºC. Unfortunately, the thermal stability of CO_2/SO_2 is not yet confirmed, but experimental analysis is currently underway. However, previous studies in the literature have indicated that CO_2/SO_2 is thermally stable at temperatures above 700 ℃ [11].

In addition to thermal stability, environmental hazards have been considered for the selected mixtures. $TiCl_4$ has potential limitations due to its high reactivity with moisture in the air and the formation of HCl and TiO_2 when combined with water which are both hazardous to human health. For these reasons the current study seeks to optimise the turbine flow path design for a CO_2/SO_2 pre-compression cycle layout. The sCO_2-SO_2 mixture is found to be promising to increase the cycle thermal efficiency. Considering environmental hazards, the optimum cycle performance, and thermal stability a molar mixture of 80% CO_2 and 20% SO_2 is used.

Research has determined that turbine performance influences the thermal efficiency of sCO_2 cycles considerably [12-14]. A study by Novales et al. [12] estimated that sCO_2 cycles can only compete with state-of-the-art steam cycles if turbine efficiencies are above 92%. They also estimated that a 1% efficiency change in turbine could result in 0.31-0.38% change in cycle efficiency. However, according to Allison et al. [14], a 1% decrease in turbine efficiency could decrease cycle efficiency by 0.5%. Therefore, it's evident that the path to commercial realization of sCO_2 cycles entails a better understanding of turbine design; yet it remains to be seen what effect CO_2 mixtures have.

Several authors have investigated the design of sCO_2 turbines of varying scales to reveal critical design considerations and the expected range of efficiencies. Zhang et al. [15] conducted a CFD analysis on a 15 MW single-stage axial turbine, predicting a total to static efficiency of 83.96%. The study also demonstrated the significance of gas bending stresses on the turbine blades, did not investigate the benefit of adding additional stages to turbine performance. On the other hand, Shi et al. [16] predicted a total-to-total efficiency of 92.12% for a a three-stage design for a 10 MW_e axial turbine. Moreover, they showed that the turbine can maintain 85% to 92% efficiency while operating at off-design conditions in the range of mass flow rate from 115 kg/s to 201.3 kg/s. Total-to-total efficiency above 90% were also predicted by Bidkar et al. [17] for 4-stage and 6-stage 50 MW_e and 450 MW_e axial turbines, respectively. Kalra et al. [18] designed a four-stage axial turbine for a 10 MW CSP plant. The study focused on practical considerations such as mechanical integrity, vibrational damping, sealing, shaft assembly, and operational transients. It highlighted the unique challenges imposed by sCO_2 turbines such as high torque transmission

requirements, small aerofoil design and fabrication, aero-design optimisation with mechanically safe blade design, and high cycle fatigue life of the rotor. Vane et al. [19] designed the first stage of a sCO_2 axial turbine by mean-line design and 3D design using STAR-CCM+ CFD package. They found that both methods predict similar vane geometries, but mean-line design overestimates the efficiency of the stage when compared to the CFD analysis. The reason for the discrepancy was attributed to the inadequacy of Soderberg loss calculations to capture all primary losses. They also observed that the fluid's high density at turbine inlet results in short blades relative to the blade chord length, which promote secondary flow and tip clearance losses. Additionally, the loading coefficient was found to be high enough to warrant a 6-stage turbine.

The turbine design process in the current study is initiated using thermodynamic models which generate the basic geometrical parameters, usually known as a mean-line design [20], and finalised through 3D numerical modelling and simulation to match the cycle requirements and seek the best performance [21]. To properly model the thermodynamic properties of the selected CO_2 mixtures, Aqel, et al. [22] investigated the effect of the choice of the equation of state (EoS) and its calibration on the turbine design accuracy. The uncertainty in mean diameter and blade height when using the Peng-Robinson EoS were 2.6% and 4.3%, respectively. This indicates that turbine designs for CO_2/SO_2 can be designed with reasonable accuracy even with uncertainty in the fluid model.

Turbine blades are generated using the mean-line model analysis to create initial geometry used to set up the CFD model and initiate the aerodynamic simulation and structural analysis. A conjugate aerodynamic-structural blade shape optimisation model is then applied to improve the 3D blade design and bring the design to the required constraints informed by the power cycle [21]. Kalra, et al. [18] followed a similar methodology in designing a 4-stage sCO_2 expander through generating a mean-line flow path followed by a 3D numerical simulation and detailed rotodynamic analysis. Jang, et al. [23] verified the applicability of CFD models to simulate an ultra-supercritical 10-stage axial steam turbine, and their results proved the validity of the model compared to reference design data.

In this paper, a turbine design is presented for a 130 MW axial turbine operating with an 80-20% molar composition of sCO_2/SO_2. This design is based on both mean-line design and CFD simulation. Design constraints are introduced to ensure design feasibility including aerodynamic performance, rotodynamic analysis, and mechanical integration. These constraints are based on industrial experience which can be easily assessed and controlled throughout the mean-line design process. The performance of the turbine is evaluated at different operating points to better understand off-design performance.

DESIGN PROCESS

Mean-line design

An in-house mean-line design tool is used to develop the turbine flow path [20, 24]. Within the tool, the steady-state mass, energy, and momentum equations are solved to obtain blade geometry, velocity triangles and thermodynamic properties for all turbine stages. The design process starts by defining the boundary conditions, including the total inlet temperature, the total inlet pressure, the pressure ratio, the mass flow rate, and inlet flow angle. Six decision parameters, presented in Table 1, are defined which includes the loading and flow coefficients (ψ, ϕ), degree of reaction (Λ), trailing edge to throat ratio (t/o), pitch to chord ratio (s/c), and blade surface roughness. The values for ψ and ϕ are selected to allow for optimum turbine aerodynamic performance based on the Smith chart [25]. Trailing edge to throat ratio (t/o) is selected to reduce the trailing edge losses based on the specified range in the literature [47] and the pitch to chord ratio is selected based on an industrial recommendation.

Using the boundary conditions and the decision parameters, the number of turbine stages and the number of rotor and stator blades, $35 < n_{blades} < 100$, are defined to provide an optimised aerodynamic design complying with the mechanical and rotodynamic constraints. To ensure the mechanical integrity of the blades, the static bending stress limit is set to 130 MPa excluding any stress intensification factor (SIF) and a slenderness ratio, defined as the ratio of the total axial flow path length to the hub diameter, less than 9. At this stage, the thermodynamic properties and velocity triangles can be obtained at each design station for both the stator and rotor as defined in Figure 1. Following that, the blade geometry can be obtained including, blade heights, annulus area, chord and axial chord length, blade pitch, and throat-to-pitch ratio (o/c), as shown in Figure 2, [20, 24]. The mean-line design model generates a 1D geometry of the blades for each stage including the inlet/outlet angles, the stagger angle, the chord length, the throat opening, and the trailing edge thickness. The flow path radii at the hub/tip, the number of stages, the number of blades per stage, and the tip clearance values are also provided.

Table 1 Mean-line model design criteria

Design parameter	Value	Design parameter	Value
Surface roughness [mm]	0.002	Degree of reaction Λ [-]	0.5
Stage flow coefficient ϕ [-]	0.5 [25]	Trailing edge thickness to throat ratio t/o [-]	0.05 [26]
Stage loading coefficient ψ [-]	1 [25]	Pitch-to-chord ratio s/c [-]	0.85 [27]

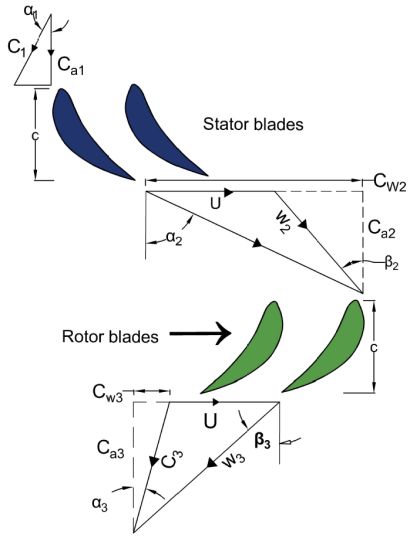

Figure 1 Geometry of a blade section

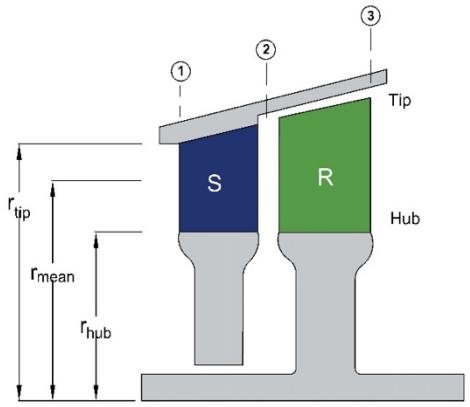

Figure 2 Axial flow turbine stage showing the stator (S) and the rotor (R).

According to an analysis conducted by the authors in a previous work, the Aungier loss model [28] is one of the most suitable for sCO_2 axial turbine design [24]. The mean-line design tool has been previously verified against multiple cases from the literature. This includes cases involving air, sCO_2 and ORC as working fluids. A good agreement was obtained for both the geometric parameters as well as the total-to-total efficiency. A maximum percentage difference of 1.5% and 1.2% in the total-to-total and total-to-static efficiency, respectively, was observed.

Numerical model

The turbine design process is initiated using the mean-line design model to generate the initial 3D blade geometry [21]. A few assumptions are made at this stage to construct the initial aerofoil 2D geometry, such as leading-edge thickness, inlet/outlet wedge angles, aerofoil curvature control points, and blade base fillet. The 2D aerofoil is then extruded to form the 3D blade since the mean-line design indicates relatively short blades. More specifically, the ratio of the blade height to the mean diameter ranges between 8% and 15%. A CFD simulation is then completed for the proposed geometry and the CFD results are compared against the mean-line design model. To ensure a suitable design, the predicted mass flow rate for the given pressure ratio is compared with cycle design requirements and the 3D blade design assumptions are adjusted accordingly. The resulting 3D blade geometry is then evaluated FEA to ensure mechanical stresses are within the imposed limits, where the blade base fillet is adjusted to satisfy the stress constraints. Further improvements to the 3D blade geometry are achieved using blade shape optimisation with the goal of matching the cycle operating conditions while improving performance.

A 3D steady-state multi-stage CFD model is setup for a single flow passage, as shown in Figure 3. The turbulence model is k-ω SST, which is widely considered for turbomachinery simulations [29]. Near the walls, a scalable wall function model is used, which employs equilibrium wall functions for high Reynold's number flow. The CFD solver used is ANSYS CFX (2020 R2). The interfaces between the stator and rotor blades are modelled using a mixing plane with pitch ratios defined as the ratio between the number of blades of the downstream blade row to the upstream blade row. In the proposed design, the ratio of the rotor to stator number of blades ranges between 0.893 to 0.914. The boundary conditions defined for this model are the total pressure and the total temperature at the inlet of the first stator blade, while the outlet is defined as the static pressure of the last rotor. The rotor tip clearance is considered 0.07% of the tip diameter for each stage.

Alongside design-point verification, an off-design CFD model is setup to assess turbine performance away from the design point and give an indication of the acceptable turndown that can be achieved without a significant deterioration in performance. The off-design simulations are setup by varying the inlet total pressure while maintaining a constant inlet total temperature and static outlet pressure.

The mesh quality has been controlled by controlling the global element size while maintaining y^+ values on the walls around 50 to best suit standard wall functions [30]. The final number of grid points is based on a mesh independence study applied to a single stage, as reported in Figure 4, targeting efficiency variation within 0.02% compared to the finest mesh. This mesh size is then generalised to the remaining stages. The total number of grid points per stage in this case ranges between 3.1 and 3.7 million points, while the total number of grid points of the domain is 47.3 million, which is sufficiently large to capture the fine flow vortices and better approximate the turbine performance.

The thermo-physical properties of the sCO_2 mixtures are evaluated using SIMULIS[31]. The selected equation of state is Peng Robinson in both mean-line design and CFD simulations, for its simplicity and accuracy [22]. The binary interaction parameters for the selected EoS were selected to match those used for the cycle analysis to ensure consistency in the thermodynamic properties obtained by both models [22, 32]. The properties are introduced to the CFD models using look-up tables that cover the expected pressure and temperature ranges with the size of 500×500 points.

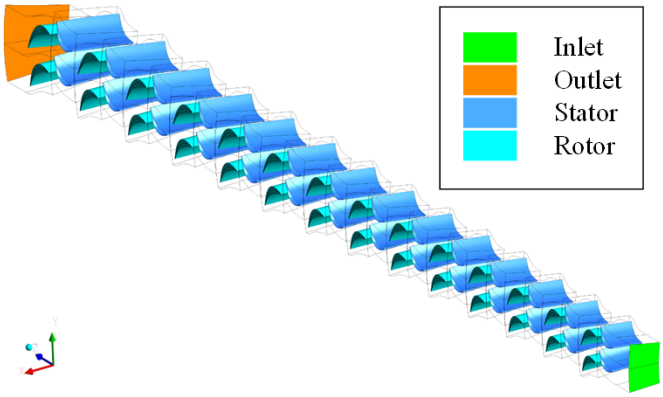

Figure 3 Numerical model domain of the 14-stages

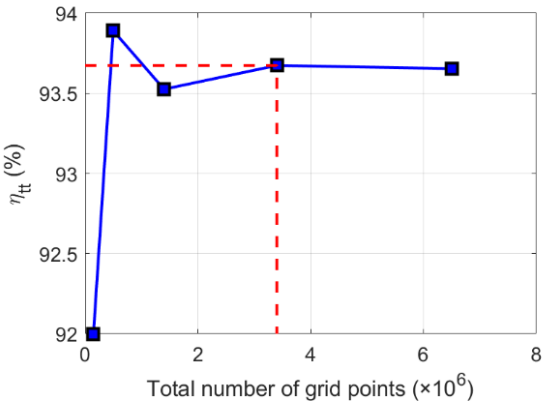

Figure 4 Mesh study of a single stage out of the 14-stage design

Blade shape optimisation

The 3D blade geometry, extruded from the 2D profile, can be further improved through blade shape optimisation as explained by the authors in a previous publication [21]. The optimisation model uses a set of decision variables represented by the blade aerofoil geometry while the objectives and constraints are introduced to maintain efficient operation and a safe design. The search space is defined by selecting a certain range for the different geometrical parameters defining the blade shape such as the thickness and angle magnitudes at different locations as shown in Figure 5. The range for each decision variable is defined around the reference value by manual iterations aimed at maintaining a reasonable aerofoil shape as reported in Figure 6. The figure shows the minimum (Min) and maximum (Max) values for the stator thickness (St) and angle (Sa), relative to the reference (Ref) value. The four points given on the x-axis correspond to the Leading edge, mid-point 1, mid-point 2, and trailing edge as defined in Figure 5.

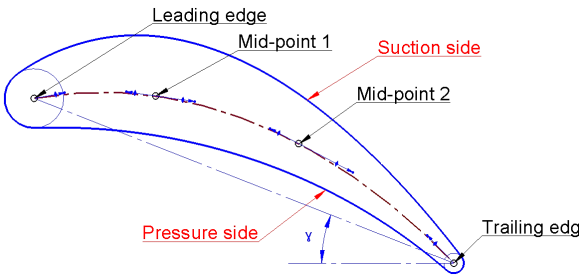

Figure 5 Blade aerofoil geometry as defined for the optimisation model

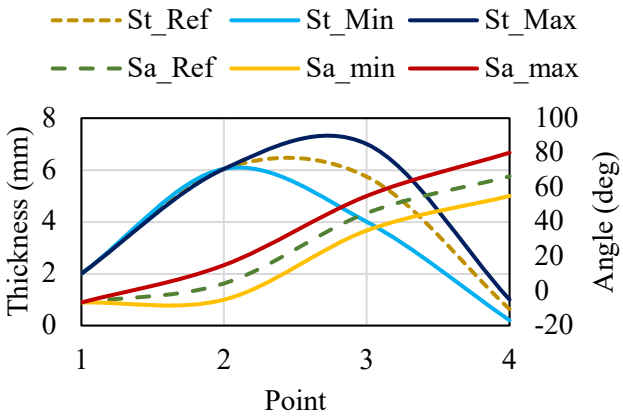

Figure 6 Exemplary range for decision variables of optimisation model search space

Within the optimisation model, the mass flow rate is confined to within 1% of the cycle design mass flow rate and the maximum stress is kept under 260 MPa. This stress limit accounts for all stress and is not to be confused with the static stress limit imposed in the mean-line design as the former limit represents the peak equivalent stress while the latter limit is an average cross-section stress.

A genetic algorithm (GA) is used for optimisation. It starts by defining a set of initial solutions, which are evaluated using the CFD/FEA models and are assessed based on the fitness criteria such as mass flow rate, efficiency, and peak stresses. A one-way link is set up where the CFD flow results are transferred to the FEA model to define the aerodynamic loads. Due to the limited blade deformation, which is found to be within 0.2% of the blade height, there is considered limited added value in studying the effect of blade generation of the flow field. The details of the GA model are described in the authors' previous work [21]. Once the solutions are evaluated, the GA performs selection and recombination processes to generate the new generation of solutions. This process is repeated until one of the termination criteria is met, such as the maximum number of iteration or a certain tolerance. The optimisation carried out on a surrogate model to replace the physical CFD/FEA models during the optimisation iterations as reported by in [21]. Although this methodology depends on the surrogate model accuracy, it allows for increasing the number of iterations during the optimisation process and achieving lower tolerance. The mutation and crossover probabilities can also be increased with a large population size, reducing the risk of convergence to a local optimum solution [33].

RESULTS AND DISCUSSION

Flow path design

A 130 MW axial turbine is designed based on the boundary conditions and cycle requirements selected for the SCARABEUS project. A summary of the boundary and operating conditions is reported in Table 2. The turbine is designed to produce 130 MW power, corresponding to for a 100 MW_e net CSP plant. The turbine rotational speed is fixed at 3,000 RPM to match the electrical grid frequency requirements (i.e., 50 Hz) since it is not practical to use a gearbox to decouple turbine and generator speed at such power scales. Initially, the aerodynamic performance of a 4-stage design was investigated, which was intended to limit the peripheral speed of the shaft to 180 m/s. That design achieved a total-to-total efficiency of 87.5%, as evaluated by the mean-line loss model. To enhance the performance, the number of stages has been increased, whilst constraints have been introduced to ensure the rotor static bending stress is less than 130 MPa for all stages, for rotor blades count ranging between 35 and 95, and the slenderness ratio less than 9. In view of the fact that turbine designs were evaluated at a constant rotational speed and loading coefficient of 3000 RPM and 1.0, respectively, [24], the number of stages dictated the peripheral blade speed and hence the hub diameter based on the isentropic enthalpy drop for the CO_2/SO_2 mixture. Increasing the number of stages resulted in smaller peripheral speed and hub diameter yielding to a higher total-to-total efficiency as indicated in Figure 7.

Table 2 Boundary and operating conditions

Parameter	Value	Parameter	Value
Dopant	SO_2	Turbine outlet static pressure [bar]	81.24
Dopant molar fraction [%]	20%	Mass flow rate [kg/s]	827
Turbine inlet total pressure [bar]	239	Rotational speed [RPM]	3000
Turbine inlet total temperature [K]	973		

As a result of such design factors, the number of stages can be increased up to 14-stages without exceeding the maximum rotoric bending stress and slenderness ratio limits. Increasing the number of stages from 4 to 14 results in an increase in total-to-total efficiency of 6.3%, thus achieving a design total-

to-total efficiency of 93.8% as evaluated by the mean-line loss models; this is due to the reduction in peripheral speed from 194 to 107 m/s, and hub diameter reduction from 1.2 to 0.62 m. The 14-stage design has a flow path length of 1.8 m, although the total shaft length including the bearing span and axial gaps larger. The meridional cross section of the turbine flow path is shown in Figure 8, where the unfilled and filled shapes represent the stator and rotor blades respectively. Representative geometrical parameters for the preliminary flow path, as obtained using the mean-line design model, are reported in Table 3.

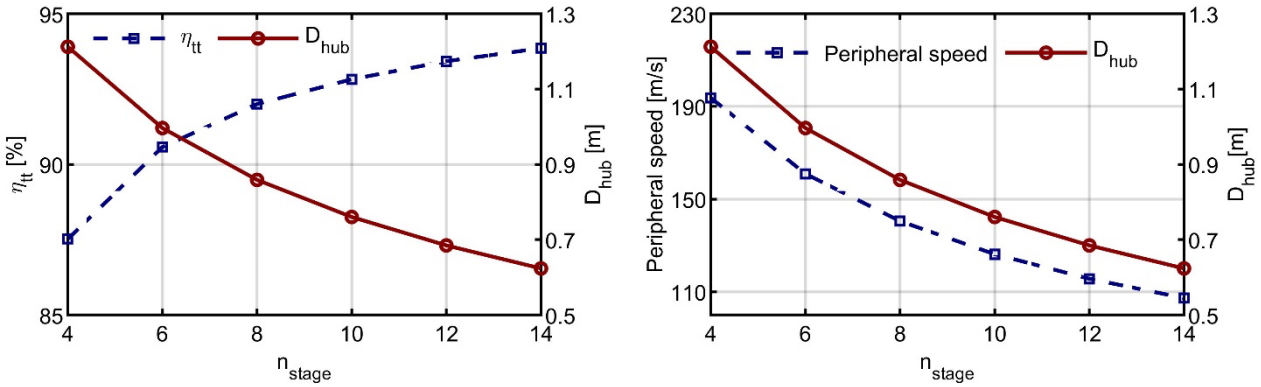

Figure 7 Effect of the number of stages (n_{st}) on the total-to-total efficiency (η_{tt}), hub diameter (D_{hub}) and peripheral speed for the CO_2-SO_2 mixture as evaluated by the mean-line loss model

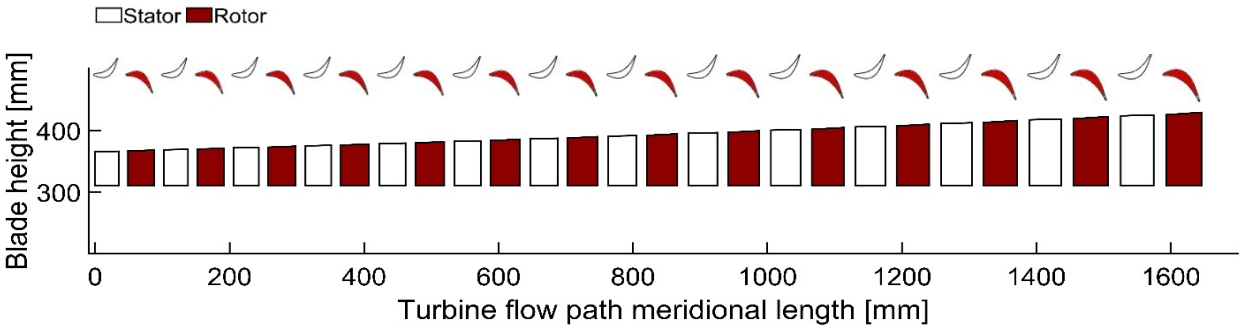

Figure 8 Proposed flow path design meridional view

Table 3 Mean-line turbine design data for the 1st, 7th, and 14th stages.

	S1	R1	S7	R7	S14	R14
Axial chord [mm]	35.53	38.96	40.43	44.28	48.75	53.12
Hub radius [mm]			310.61			
Inlet tip radius [mm]	365.17	366.54	386.34	387.54	423.51	425.21
Outlet tip radius [mm]	366.17	368.04	387.21	389.81	424.74	428.99
No. of blades	58	53	53	48	47	42
Tip gap [mm]	-	0.515	-	0.546	-	0.601

Following the preliminary mean-line design, the 3D numerical model is setup based on the provided design parameters with the boundary and operating conditions reported in Table 2. The CFD numerical results are compared to the cycle requirements while several design parameters such as the outlet wedge angle, the inlet/outlet fillet radius, and the suction side (SS) curvature control points are manually adjusted to control the throat opening and the mass. The results of the modified geometry are compared to the mean-line design (MLD) results in **Error! Not a valid bookmark self-reference.**. The deviations from the mean-line design are 0.51%, 1.38%, and 0.52% in mass flow rate, power, and total-to-total efficiency, respectively.

Table 4 Comparison between mean-line design and CFD model results

Parameter	Unit	MLD	CFD	Difference
$\dot{m}$	kg/s	827.06	822.9	0.51%
$Power$	MW	131.9	130.1	1.38%
η_{tt}	%	93.84	92.90	1.01%
η_{ts}	%	93.06	91.95	1.21%

The mass flow averaged relative Mach number at the exit from each blade row is compared between the CFD and the mean-line design results in Figure 9. Overall, both models show the same trend where the Mach number increases as the flow moves through the turbine, which is due to the pressure, temperature, and speed of sound reducing along the expansion progress. Results from the mean-line agree with those from the CFD models, however the velocities predicted using the CFD model tend to be slightly higher within the final stages due to cumulative differences between the models. The difference between the flow distribution of the first and last turbine stages at the design point are compared on a mid-span plane in Figure 10. The average stage Mach number is higher in the last stage compared to the first stage. However, both stages exhibit a smooth flow from left to right without any obvious separation vortices.

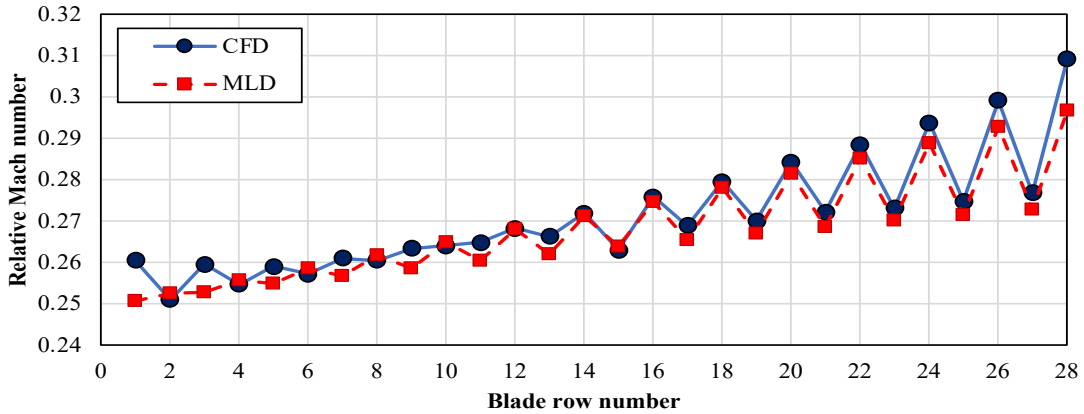

Figure 9 Exit Mach number from each blade row obtained using the mean-line design and CFD

As a final step in the initial 3D blade design process, the peak stresses are analysed on the first and last turbine stages. These stages are chosen because the first stage have the highest pressure and

temperature, while the last stage have the longest blades so, they experience the most critical bending stresses. Initial adjustments are made to the design such as increasing the outlet wedge angle, increasing the base aerofoil thickness, increasing the whole blade thickness, or increasing the base fillet size to bring the peak stresses under 260 MPa. The effect of the prementioned parameters for the first turbine stage are summarised in Table 5. Similar trends were obtained for the last turbine stage.

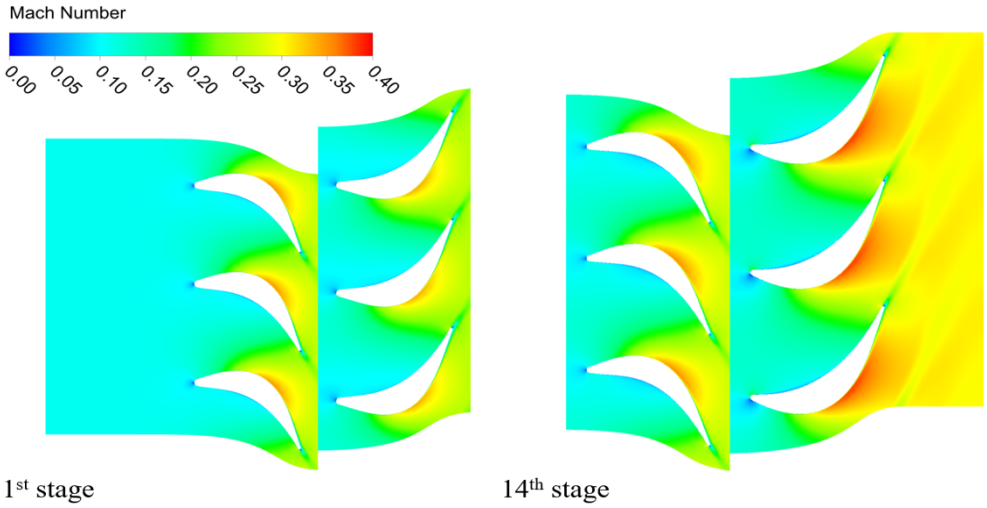

Figure 10 Comparison between the flow-field obtained for the 1st and 14th stage at the design point

Table 5 The effect of geometry tuning on the peak stresses and aerodynamic performance

Model	$\dot{m}$	$Power$	η_{tt}	σ_S	σ_R
Reference geometry	898.22	10.07	93.15	445.70	310.64
Increase outlet wedge angle, (throat opening decrease 5%)	846.46	9.60	92.98	333.28	258.38
Increase the base aerofoil thickness (around 25%)	873.38	9.76	92.77	272.13	237.99
Increase the whole blade thickness (around 25%)	848.72	9.46	92.19	269.86	223.97
Increase base fillet radius from 1 mm to 2 mm	890.15	9.85	92.86	238.36	264.22

Further improvements to the blade geometry are achieved through blade shape optimisation. This design phase seeks to improve the performance within the system constraints, however the performance improvement achievable through blade shape optimisation depends on how the reference geometry performs, and how flexible the model constraints are. A comparison between a sample reference and optimised turbine stage are shown in Figure 11 where the axis represents the axial (Z) and tangential (T) directions, while the radial direction is selected at mid-span. The results of blade shape optimisation have shown an increase in the total-to-total efficiency from 90.2% obtained from the initial blade model to 92.9% for the optimised geometry. The optimised geometry for the first stage shows only slight variations when compared to the last stage. This is because turbulence is much lower at the turbine inlet compared to the cumulative vortices and incidence effects that occur due to flow deviation within the final stage. As a result, the inlet wedge angle is significantly increased in the last stage from 15° to 26° to account for the

larger flow angle deviation from the blade angle and reduce flow separation. This modification in last stage has resulted in an increase to the total-to-total efficiency relative to the reference geometry of 0.65% more than the improvement achieved for the first stage for the same reference blade assumptions.

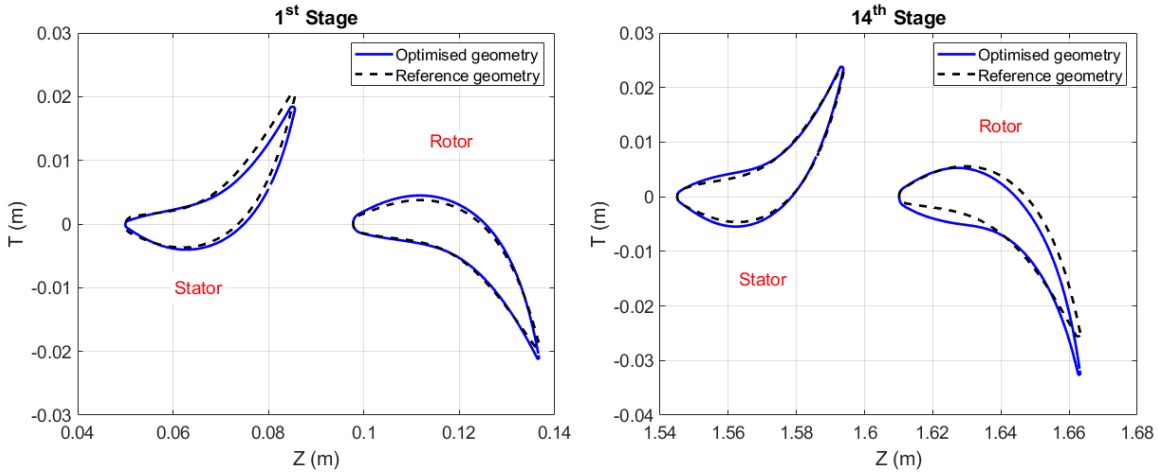

Figure 11 Comparison between reference and optimised aerofoil for the 1st and 14th stage.

Evaluation of design-point performance

The performance of each turbine stage is evaluated using both mean-line design and CFD models as summarised in Figure 12. A good agreement was obtained between both models for both total-to-total and total-to-static efficiencies; however, the mean-line loss model predicts a lower total-to-total efficiency than the CFD for most of the stages with an average difference of 1.2% across the stages. The overall trend indicates a slight increase in the total-to-total efficiency with the stage number. It can be observed that the difference between the total-to-total and total-to-static efficiency is high for each single stage, as reported in Figure 12, and low for the multi-stage calculation as reported in Table 4. This is because the exit kinetic energy from a single stage is approximately equal to the exit kinetic energy from the whole turbine. However, the ratio between the exit kinetic energy to enthalpy drop is much lower for the multi-stage calculation compared to a single stage. As such, the difference between total-to-total to total-to-static efficiency due to the exit velocity is around 1% for the entire turbine, compared to 10% for a single stage.

Investigation of the loss breakdown structure of similar turbine stages has revealed that end-wall losses are the predominate aerodynamic loss in turbines of this scale operating within sCO_2 [24]. However, near the final turbine stages, where the blades are longer and the boundary layers occupy a narrower portion of the flow path, the overall losses are lower. Similar to the total-to-total efficiency, the total-to-static efficiency decreases almost in unison with the shift in the total-to-total efficiency, which is because all the stages are designed with identical velocity triangles. To further understand the distribution of losses between the turbine stages, the enthalpy loss coefficients obtained using the CFD model results are plotted over the efficiency curves in Figure 12. Generally, the losses decrease with the stage number, which reflects the efficiency results shown in Figure 12. Moreover, the rotor losses are higher than the stator losses due to the blade rotation and tip clearance which generates more turbulence. However, the last stator and rotor enthalpy loss coefficients are 39% and 13% lower than the first stage, respectively. This indicates that the rotor losses are more affected by the development of the flow field and cumulative flow angle deviation compared to the stator losses.

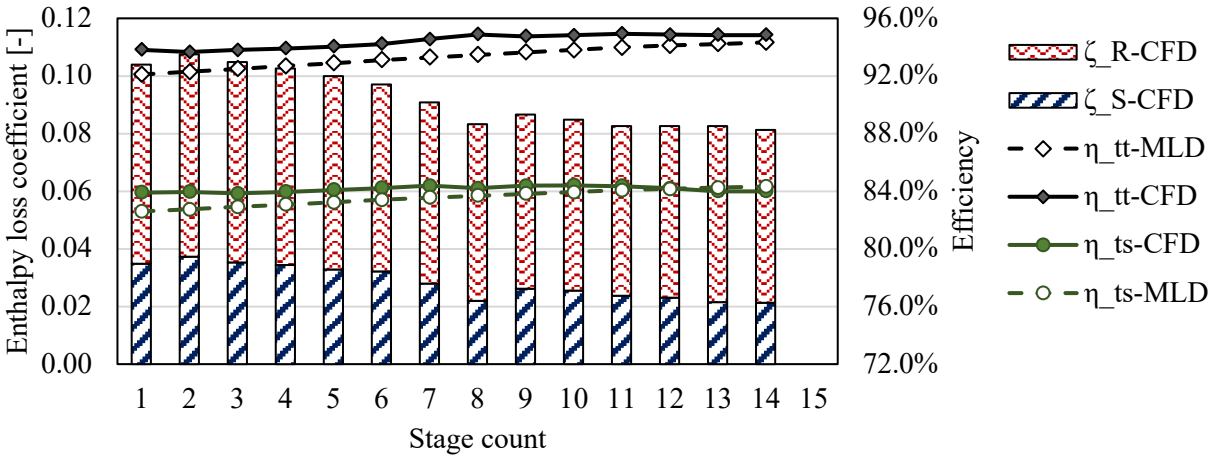

Figure 12 Comparison between the MLD and CFD total-to-total and total-to-static efficiencies per stage along with the enthalpy loss coefficients obtained using the CFD model results

Off-design analysis

The performance of the turbine at off-design has been investigated using the CFD model and the results are reported in Figure 13. Varying the pressure ratio shows an almost linear relation with the mass flow rate over most of the tested operating range. The total-to-total efficiency is effectively constant between 90% and 130% of the design mass flow rate, but reduces at lower mass flow rates. The turbine can operate down to 50% and 40% of the design mass flow rate with total-to-total efficiencies of over 80% and over 60% respectively. A further reduction in the mass flow rate leads to a poor turbine performance or even a negative power output, which indicates that the turbine is performing as a compressor and requires external power to continue running.

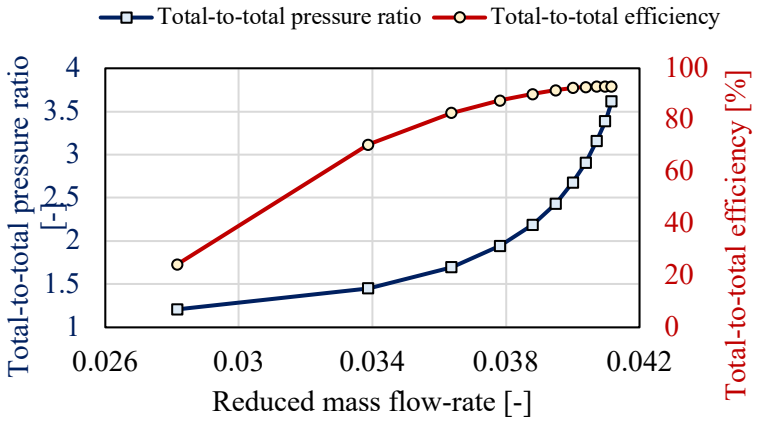

Figure 13 The off-design performance maps of the proposed turbine design

The power produced by each stage at different off-design operating points is reported in Figure 14. At the design inlet pressure of 240 bar, the power produced by each stage is almost the same, as expected for a repeating stage design. However, higher or lower inlet pressures results in a non-uniform power generation per stage. At higher mass flow rate operating conditions, the stage power increases with stage number as a result of increasing absolute velocity magnitudes, which assuming the same blade outlet angles increases both axial and tangential components. When the velocity increases the fluid density must

also decrease, which further compounds this increase in velocity. As such the velocity and power increases from stage to stage until reaching a peak value for the last stage. In contrast, at low mass flow rates the velocity decreases and density increases, leading to an accumulative velocity and power decrease until reaching a minimum power for the last stage. The performance at low inlet pressure (i.e., 120 bar) shows almost zero power output from the last stage which means that this stage is no longer driving the turbine, which causes a sharp drop in overall turbine efficiency. The expansion diagram represented by the enthalpy-entropy plane is reported in Figure 15 which reflects the observations of Figure 14 and indicates the excessive entropy generation for inlet total pressures of 120 and 160 bar.

The flow deviation angle at the rotor inlet is shown in Figure 16. It can be seen that the deviation angle at the design point is around zero, such that the incidence losses are minimised. At higher inlet pressures (i.e., larger mass-flow rates), the deviation angle increases, especially for downstream stages, however the efficiency drop is negligible because no flow separation occurs. At lower inlet pressures (i.e., lower mass-flow rates), the incidence deviation angles become much higher and negative (in the clockwise direction relative to the axial direction) causing flow separation and a significant deterioration in overall turbine performance.

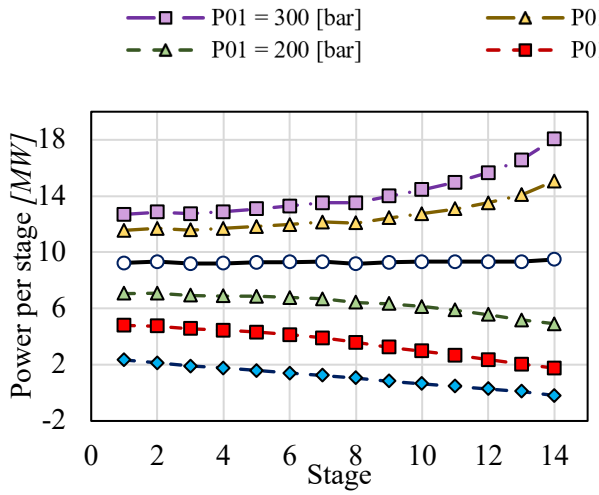

Figure 14 Power distribution per stage obtained at different operating inlet pressures

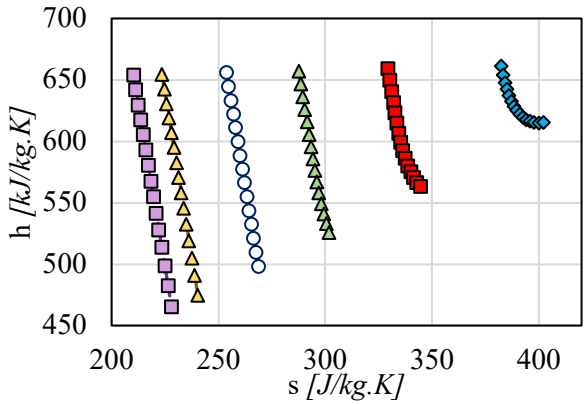

Figure 15 *h-s* diagram for different operating points whith variable inlet total pressure

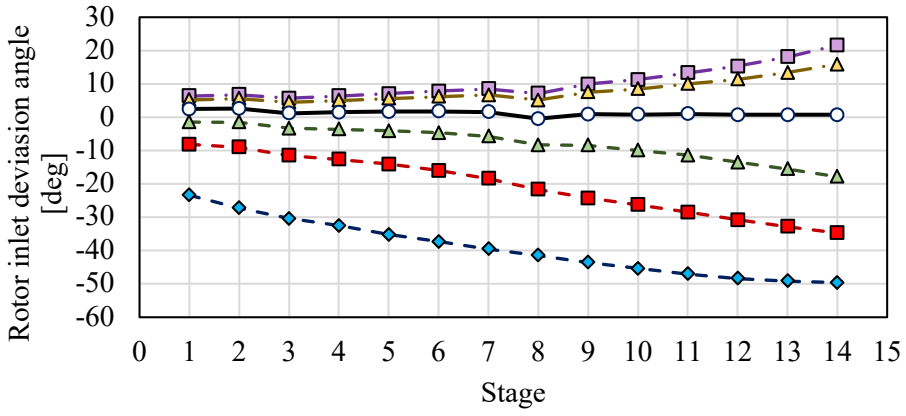

Figure 16 Off-design deviation angle at the inlet of each rotor stage

The flow structure at 100% and 50% of the design mass flow rate is represented by the Mach number distribution in Figure 17. At the design mass flow rate, the flow passes smoothly through each turbine stage, without generating any excessive vortices. Conversely, at low mass flow rate, there is an indication of flow separation towards the final turbine stages as a result of increasing the incidence angle at low mass flow rates. It has been found that the location where separation first occurs moves further upstream towards the turbine inlet as the mass flow rate is decreased. This explains the drop in efficiency and in stage power production at lower mass flow rates as shown in Figure 13 and Figure 14.

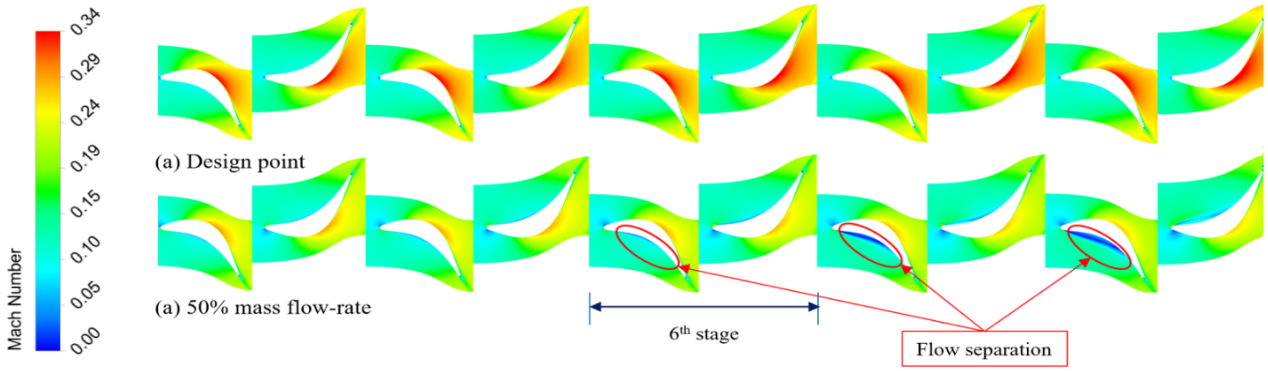

Figure 17 Flow field obtained for the five mid-stages: (a) 100% and (b) 50% design mass flow rate

Turbine Design Remarks

CONCLUSIONS

This paper presented the aerodynamic design of a 14-stage 130 MW turbine operating with a CO_2/SO_2 mixture. The design process was initiated by defining the aerodynamic and mechanical constraints along with the required cycle boundary conditions, which were used to obtain the basic flow path through mean-line design.

A multi-stage mean-line design script has been adopted based on the Aungier loss model to predict the turbine performance, which has previously been verified against the literature with maximum deviations in total-to-total efficiency of 1.5%. The mean-line results indicate that increasing the number of stages from 4 to 14 increased total-to-total efficiency by 6.3%, from 87.5% to 93.8%. Increasing the number of stages leads to a smaller hub diameter, longer flow path, and taller blades, which introduces challenges related to the shaft stability. The high gas density also leads to high bending stresses.

A good agreement has been achieved between the mean-line approach and the CFD where it can be concluded that there is no specific impact of the working fluid on the design methodology however, the working fluid impact the design assumptions and constraints. The mean-line flow path then formed the basis of the 3D blade design which was simulated and refined through 3D steady-state numerical simulation. The difference between total-to-total efficiency of the mean-line design and the CFD model was less than 2%, providing confidence in the mean-line methodology.

Alongside the initial 3D simulation, blade shape optimisation helped to further match the turbine boundary conditions with the required cycle constraints by maintaining the mass flow rate within 1% of the cycle mass flow rate for the given pressure ratio, while improving the performance by 2.7% from 90.2% to 92.9% and meeting safety and operational constraints. The performance analysis of the proposed

turbine revealed that stage losses decrease with stage number because of the accompanying increase in blade height. The last stator and rotor enthalpy loss coefficients were calculated to be 39% and 13% less than the first stage enthalpy loss coefficients, respectively.

Finally, the performance maps indicate the proposed turbine can to run down to 50% and 40% of the design mass flow rate with total-to-total efficiencies over 80%, and over 60%, respectively. Ultimately, this paper has demonstrated the suitability of the proposed methodology in designing an axial turbine for the proposed cycle that satisfies the cycle requirements at both design and off-design operating conditions whilst achieving a total-to-total efficiency of 92.9% and meeting the necessary mechanical and rotordynamic constraints. Further design activities related to the turbine assembly, such as sealing, bearings, casing design, and shaft assembly, are underway.

REFERENCES

[1] White, M. T., Bianchi, G., Chai, L., Tassou, S. A., and Sayma, A. I., 2021, "Review of supercritical CO_2 technologies and systems for power generation," Applied Thermal Engineering, 185, p. 116447. 10.1016/j.applthermaleng.2020.116447

[2] Yin, J. M., Zheng, Q. Y., Peng, Z. R., and Zhang, X. R., 2020, "Review of supercritical CO_2 power cycles integrated with CSP," International Journal of Energy Research, 44(3), pp. 1337-1369. 10.1002/er.4909

[3] Binotti, M., Marcoberardino, G. D., Iora, P., Invernizzi, C., and Manzolini, G., "Scarabeus: Supercritical carbon dioxide/alternative fluid blends for efficiency upgrade of solar power plants," Proc. AIP Conference Proceedings, AIP Publishing LLC, p. 130002. 10.1063/5.0028799

[4] Meng, F., Wang, E., Zhang, B., Zhang, F., and Zhao, C., 2019, "Thermo-economic analysis of transcritical CO_2 power cycle and comparison with Kalina cycle and ORC for a low-temperature heat source," Energy Conversion Management, 195, pp. 1295-1308. 10.1016/j.enconman.2019.05.091

[5] Binotti, M., and Manzolini, G., "Supercritical carbon dioxide/alternative fluids blends for efficiency upgrade of solar power plant," Proc. 3rd Euroepan supercritical CO_{-2} conference, September 19-20, 2019, Paris, France, DEU, pp. 141-149. hdl.handle.net/11311/1154065

[6] Tafur-Escanta, P., Valencia-Chapi, R., López-Paniagua, I., Coco-Enríquez, L., and Muñoz-Antón, J., 2021, "Supercritical CO_2 Binary Mixtures for Recompression Brayton s-CO_2 Power Cycles Coupled to Solar Thermal Energy Plants," Energies, 14(13), p. 4050. 10.3390/en14134050

[7] Manzolini, G., Binotti, M., Morosini, E., Sanchez, D., Crespi, F., Marcoberdino, G. D., Iora, P., and Invernizzi, C., "Adoption of CO_2 blended with C_6F_6 as working fluid in CSP plants," Proc. AIP Conference Proceedings, AIP Publishing LLC, p. 090005. 10.1063/5.0086520

[8] Crespi, F., de Arriba, P. R., Sánchez, D., and Muñoz, A., 2022, "Preliminary investigation on the adoption of CO_2-SO_2 working mixtures in a transcritical Recompression cycle," Applied Thermal Engineering, 211, p. 118384. 10.1016/j.applthermaleng.2022.118384

[9] Crespi, F., Martínez, G., Rodriguez de Arriba, P., Sánchez, D., and Jiménez-Espadafor, F., "Influence of working fluid composition on the optimum characteristics of blended supercritical carbon dioxide cycles," Proc. Turbo Expo: Power for Land, Sea, and Air, June 7–11, 2021, Virtual, Online, American Society of Mechanical Engineers, p. V010T030A030. 10.1115/GT2021-60293

[10] Crespi, F., de Arriba, P. R., Sánchez, D., Ayub, A., Di Marcoberardino, G., Invernizzi, C. M., Martínez, G., Iora, P., Di Bona, D., and Binotti, M., 2022, "Thermal efficiency gains enabled by using CO_2 mixtures in supercritical power cycles," Energy, 238, p. 121899. 10.1016/j.energy.2021.121899

[11] Schubert, D., 2000, "Boron oxides, boric acid, and borates," Kirk-Othmer Encyclopedia of Chemical Technology, pp. 1-68. 10.1002/0471238961

[12] Novales, D., Erkoreka, A., De la Peña, V., and Herrazti, B., 2019, "Sensitivity analysis of supercritical CO_2 power cycle energy and exergy efficiencies regarding cycle component efficiencies for concentrating solar power," Energy Conversion Management, 182, pp. 430-450. 10.1016/j.enconman.2018.12.016

[13] Dostal, V., Driscoll, M. J., and Hejzlar, P., 2004, "A supercritical carbon dioxide cycle for next generation nuclear reactors," Doctor of Science, Czech Technical University, Prague, Czech Republic.

[14] Brun, K., Friedman, P., and Dennis, R., 2017, "Turbomachinery," Fundamentals and applications of supercritical carbon dioxide (sCO_2) based power cycles, Woodhead publishing, pp. 147-215.

[15] Zhang, H., Zhao, H., Deng, Q., and Feng, Z., "Aerothermodynamic design and numerical investigation of supercritical carbon dioxide turbine," Proc. Turbo Expo: Power for Land, Sea, and Air, American Society of Mechanical Engineers, p. V009T036A007. 10.1115/GT2015-42619

[16] Shi, D., Zhang, L., Xie, Y., and Zhang, D., 2019, "Aerodynamic design and off-design performance analysis of a multi-stage S-CO_2 axial turbine based on solar power generation system," Applied Sciences, 9(4), p. 714. 10.3390/app9040714

[17] Bidkar, R. A., Mann, A., Singh, R., Sevincer, E., Cich, S., Day, M., Kulhanek, C. D., Thatte, A. M., Peter, A. M., Hofer, D., and Moore, J., 2016, "The 5th International Symposium-Supercritical CO_2 Power Cycles Conceptual Designs of 50MW e and 450MW e Supercritical CO_2 Turbomachinery Trains for Power Generation from Coal. Part 1: Cycle and Turbine."

[18] Kalra, C., Hofer, D., Sevincer, E., Moore, J., and Brun, K., "Development of high efficiency hot gas turbo-expander for optimized CSP supercritical CO_2 power block operation," Proc. The Fourth International Symposium—Supercritical CO_2 Power Cycles (sCO_2), Citeseer, pp. 1-11.

[19] Schmitt, J., Willis, R., Amos, D., Kapat, J., and Custer, C., "Study of a supercritical CO_2 turbine with TIT of 1350 K for Brayton cycle with 100 MW class output: aerodynamic analysis of stage 1 vane," Proc. Turbo Expo: Power for Land, Sea, and Air, June 16 – 20, 2014, Düsseldorf, Germany, American Society of Mechanical Engineers, p. V03BT36A019. 10.1115/GT2014-27214

[20] Salah, S. I., Khader, M. A., White, M. T., and Sayma, A. I., 2020, "Mean-line design of a supercritical CO_2 micro axial turbine," Applied Sciences, 10(15), p. 5069. 10.3390/app10155069

[21] Abdeldayem, A., White, M., Paggini, A., Ruggiero, M., and Sayma, A. I., 2022, "Integrated Aerodynamic and Structural Blade Shape Optimisation of Axial Turbines Operating with Supercritical Carbon Dioxide Blended with Dopants," Journal of Engineering for Gas Turbines Power, p. 144(110): 101016 (101012 pages). 10.1115/1.4055232

[22] Aqel, O., White, M., and Sayma, A., "Binary interaction uncertainty in the optimisation of a transcritical cycle: consequences on cycle and turbine design," Proc. 4th European sCO_2 Conference for Energy Systems: March 23-24, 2021, Online Conference, pp. 164-176. 10.17185/duepublico/73942

[23] Jang, H. J., Kang, S. Y., Lee, J. J., Kim, T. S., and Park, S. J., 2015, "Performance analysis of a multi-stage ultra-supercritical steam turbine using computational fluid dynamics," Applied Thermal Engineering, 87, pp. 352-361. 10.1016/j.applthermaleng.2015.05.007

[24] Salah, S. I., White, M. T., and Sayma, A. I., 2022, "A comparison of axial turbine loss models for air, sCO_2 and ORC turbines across a range of scales," International Journal of Thermofluids, p. 100156. 10.1016/j.ijft.2022.100156

[25] Smith, S., 1965, "A simple correlation of turbine efficiency," The Aeronautical Journal, 69(655), pp. 467-470. 10.1017/S0001924000059108

[26] Kacker, S., and Okapuu, U., 1982, "A mean line prediction method for axial flow turbine efficiency," Journal of Engineering for Power, 104(1), pp. 111-119 (119 pages). 10.1115/1.3227240

[27] Ainley, D., and Mathieson, G., 1951, "A method of performance estimation for axial-flow turbines."

[28] Aungier, R. H., 2006, Turbine aerodynamics, American Society of Mechanical Engineers Press, New York.

[29] Abdeldayem, A., White, M. T., and Sayma, A. I., "Comparison of CFD predictions of supercritical carbon dioxide axial flow turbines using a number of turbulence models," Proc. Turbo Expo: Power for Land, Sea, and Air, American Society of Mechanical Engineers, p. V010T030A010. 10.1115/GT2021-58883

[30] Touil, K., and Ghenaiet, A., 2019, "Simulation and analysis of vane-blade interaction in a two-stage high-pressure axial turbine," Energy, 172, pp. 1291-1311. 10.1016/j.energy.2019.01.111

[31] Baudouin, O., Dechelotte, S., Guittard, P., and Vacher, A., 2008, "Simulis® Thermodynamics: an open framework for users and developers," Computer Aided Chemical Engineering, B. Braunschweig, and X. Joulia, eds., Elsevier, pp. 635-640.

[32] Morosini, E., Ayub, A., di Marcoberardino, G., Invernizzi, C. M., Iora, P., and Manzolini, G., 2022, "Adoption of the CO_2+ SO_2 mixture as working fluid for transcritical cycles: A thermodynamic assessment with optimized equation of state," Energy Conversion Management, 255, p. 115263. 10.1016/j.enconman.2022.115263

[33] Srinivas, M., and Patnaik, L. M., 1994, "Adaptive probabilities of crossover and mutation in genetic algorithms," IEEE Transactions on Systems, Man, Cybernetics, 24(4), pp. 656-667. 10.1109/21.286385

